electronics

MDPI

Article

Experimental Demonstration of Multi-Link Optical Camera Communication Using Denoising Autoencoders for IoT Applications

Huy Nguyen [1], Loc Cao Nguyen [2] and Nam Hoang Nguyen [2,*]

[1] Department of Electronics Engineering, Kookmin University, Seoul 02707, Republic of Korea; ngochuy@kookmin.ac.kr
[2] Department of Automation, School of Electrical and Electronics Engineering, Hanoi University of Science and Technology, Hanoi 100000, Vietnam; loc.nc222322@sis.hust.edu.vn
* Correspondence: nam.nguyenhoang@hust.edu.vn

Abstract

Radio frequency (RF) for wireless systems is widely installed across applications such as mobile communications, maritime networks, smart factories, and smart homes because of its easy setup compared with wired systems. Nevertheless, potential health concerns associated with exposure to RF waves have driven interest in optical camera communication (OCC) using visible light as a safer alternative. Concurrently, artificial intelligence (AI) is transforming automation and complex problem-solving across IoT, smart farming, and smart home ecosystems. In this study, we propose a Camera On–Off Keying (C-OOK) scheme that incorporates YOLO26n for multiple users, which supports light source detection and tracking, along with a denoising autoencoder (DAE) algorithm to assist the decoding process in long-range and mobile environments. This approach improves the traditional C-OOK by supporting multiple users simultaneously, increasing distances, and lowering the bit error rate (BER). Experimental results demonstrate reliable communication up to 15 m in a mobile environment.

Keywords: denoising autoencoder; IoT; YOLO26n; OCC; C-OOK; DAE

1. Introduction

IoT technologies have become increasingly integrated into various features of our daily routine, as well as smart homes, maritime communication networks, smart agriculture, and smart factories [1]. IoT enables physical objects to link to other devices through connectivity protocols that support information transmission [2]. These connectivity technologies can involve multiple entities, including IoT devices, microcontroller units (MCUs), animals, and humans, allowing them to communicate and interact automatically with minimal human interposition. In the era of Industry 4.0, IoT has become an essential system for real-time communication between people, electronic devices, and their surroundings. Nevertheless, most current conventional IoT systems (LoRa, ZigBee, Wi-Fi, and Sigfox) deploy based on radio frequency (RF) signals, raising concerns about potential health impacts [3]. Such concerns are particularly important in sensitive environments, such as schools and hospitals, where children and patients may be more vulnerable. Consequently, researchers have increasingly discovered alternative communication technologies that can reduce or eliminate the reliance on RF signals for specific requests. One good candidate is the use of visible light as a medium for wireless data transmission. Optical wireless communication (OWC)

Check for updates

Academic Editors: Ferdinando Di Martino and Dionisis Kandris

Received: 18 September 2026
Revised: 25 October 2026
Accepted: 30 October 2026
Published: 3 November 2026

Copyright: © 2026 by the authors. Licensee MDPI, Basel, Switzerland. This article is an open access article distributed under the terms and conditions of the Creative Commons Attribution (CC BY) license.

has attracted considerable attention as a substitute communication system for an RF system and can be broadly characterized into three major approaches: visible light communication (VLC), light fidelity (Li-Fi), and optical camera communication (OCC). VLC and Li-Fi typically employ photodiodes to detect signals using the power from light emitted by LEDs, whereas optical camera communication utilizes image sensors as optical receivers. Both global-shutter and rolling-shutter image sensors have been widely adopted in OCC technologies [4]. Selecting a suitable OCC scheme strongly depends on the characteristics of the image sensor used as the receiver. Compared with conventional RF technologies, OWC provides some significant advantages:

- Immunity to RF interference: Unlike RF communication, optical wireless communication (OWC) offers advantages such as immunity to RF electromagnetic interference (EMI), and visible light waves are non-EMI and safe for human health if we support non-flicker methods [5].
- Increased bandwidth: The visible light spectrum, which is available without a license, offers higher bandwidth over 1000 times that of the conventional RF spectrum, providing higher data transmission capacity and spectrum availability.
- High security: Visible light provides enhanced physical security and transmission efficiency when a line-of-sight (LOS) channel is maintained.

Based on the potential of optical wireless communication, a lot of industry companies and academic universities have promoted significant efforts toward OWC standardization, starting with the IEEE 802.15.7-2011 standard [6] for VLC and progressing to the updated IEEE 802.15.7-2018 specification [7]. Due to the advances in LED manufacturing, we may establish LEDs as an optimal next-generation optical transmission platform due to their low power consumption, long operating life, and high-frequency switching capabilities, which are necessary for high data transmission rates [8,9]. Furthermore, while RF systems generate electromagnetic interference (EMI) [10,11] with potentially adverse effects on neurological health, OWC offers an alternative to RF communication in EMI-sensitive environments due to its immunity to RF electromagnetic interference [12]. VLC and Li-Fi utilize photodiodes (PDs) as receivers to collect high-speed LED intensity modulation information [13], leveraging advanced techniques such as pulse density modulation [14,15] and multiple-input multiple-output (MIMO) architectures [16,17] to achieve ultra-high data transmission rates. However, photodiode-based OWC reveals a lot of limitations over long ranges, with a maximum distance at approximately 10 m with specialized optical lenses [18], and severe signal degradation over long distances and in outdoor environments. However, optical camera communication (OCC) employs image sensors as receivers, achieving long ranges up to 200 m [19]. The data rate of OCC depends on the camera parameters [20,21]: global-shutter cameras require frame rate and packet rate synchronization based on the Nyquist theorem, whereas rolling-shutter cameras leverage line-by-line readout speeds to achieve higher sampling rates. By controlling the camera parameters—including the camera focal length, exposure time, and signal-to-noise ratio (SNR)—OCC can reduce the effects of mobile environments and long distances due to the SNR decreasing, which is an effect that limits PD-based OWC.

Region of interest (RoI) methods allow for the tracking of multiple sources in OCC technologies. Nevertheless, RoI methods become challenging to use when rolling shutter effects produce alternating black-and-white stripe patterns across the image frame. C-OOK modulation, introduced in IEEE 802.15.7-2018 [6], provides high speed but operates at a limited distance with a high BER. Although subsequent scheme variants [22,23] incorporate matched filtering to extend communication distances and lower the BER, these approaches fail to maintain a reliable performance in mobile environments, as detailed below. In this

study, we recommend deep learning instead of the conventional algorithms for C-OOK system for long-range, multi-user mobile environments.

The rest of the paper is organized as follows: Section 2 discusses contributions of this paper. The system architecture of a denoising autoencoder for data decoding and YOLO26n for object detection are presented in Section 3. In Section 4, the long-distance implementation results based on the DAE are presented. Finally, Section 5 concludes this paper.

2. Our Contributions

This study presents deep learning for light source tracking and a DAE algorithm to assist the decoding process in a C-OOK system for multiple users. This approach aims to maximize the data throughput while minimizing the BER under challenging long-range and mobile conditions. The contributions of our work are summarized below:

- Support for the frame rate variation effect: Frame rate variation in cameras can cause packet-missing and synchronization issues between the LED and camera. To resolve this, we proposed sequence numbers (SNs) for each packet payload, allowing the system to identify the frame rate on the receiver side and the packet rate on the transmitter side.
- Missing packet detection: By applying SNs to each packet, the receiver can detect the missing packet in an undersampling case. The receiver will compare the SNs in consecutive frames. If the SNs of consecutive frames are not continued, we can be sure that the missing packet was detected.
- Merging data packets: By applying SNs to each packet, the receiver can remove the redundant packet and merge the payload packet in an oversampling case. The receiver will merge the SNs in consecutive frames and remove the repeated packet with the same SN values.
- Enhanced mobility support: C-OOK schemes work based on the rolling shutter effect and are highly sensitive to mobile environments (velocity of 0–3 m/s). The YOLO26n model supports the real-time detection and tracking of multiple LEDs, even in mobile environments.
- Increased OCC performance: By employing a lightweight denoising autoencoder (DAE) tailored to an OCC system, the proposed system can improve the decoding performance while maintaining the computational efficiency in harsh environments. From this, we can more easily decode data than when using conventional technologies.

3. System Architecture

Optical camera communication (OCC) systems transmit data by modulating the optical intensity of LEDs, relying on efficient modulation schemes to maximize the link performance. Among these techniques, OOK is the simplest and most prevalent form of amplitude-shift keying (ASK), encoding the binary "1" and "0" using optical "on" and "off" states, respectively. In this work, we present the C-OOK scheme, which deploys deep learning to perform both LED tracking and signal decoding. By applying a DL network, the proposed architecture substantially improves its communication reliability and performance compared with conventional C-OOK systems. The experimental OCC system employed an LED array (12 V, 3 W, and size of 5 cm × 5 cm) and an FL3-U3-13S2C-CS rolling-shutter camera that operated at 60 fps. The Manchester code and Hamming (15,11) were used at a 10 kHz optical clock rate. Figure 1 illustrates the overall architecture of the deep learning-assisted C-OOK modulation scheme for this IoT system.

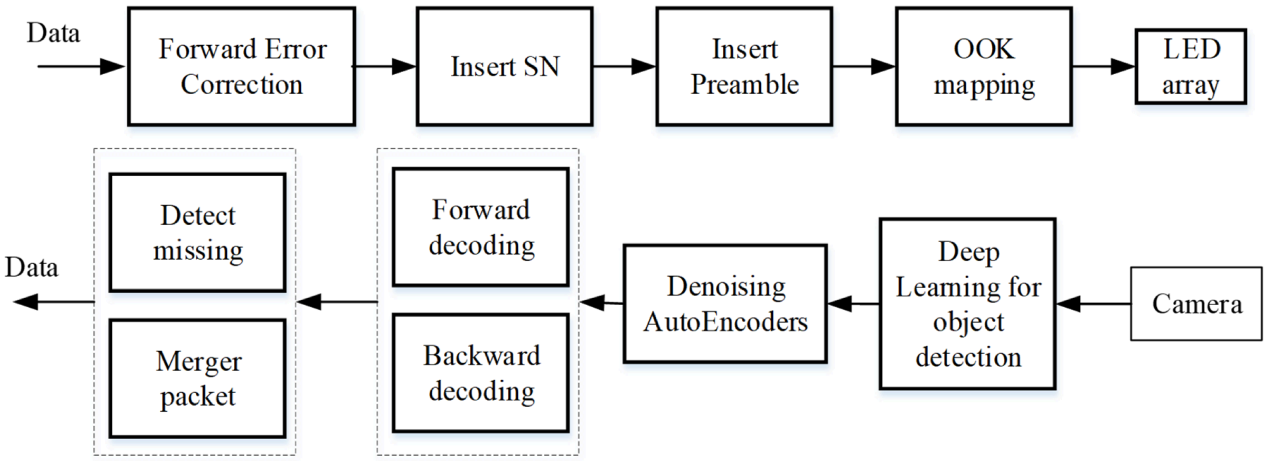

Figure 1. Deep learning-assisted C-OOK modulation scheme for our IoT system.

3.1. LED Detection Based on YOLO26n

Region of interest (RoI) algorithms are widely deployed for target detection and tracking [24–26], typically relying on feature- and object-level extraction. Nevertheless, C-OOK is used for the rolling-shutter effect, where the data are collected in the camera as alternating bright and dark stripe patterns representing the binary bits "1" and "0". The presence of many stripes in each image causes many problems for conventional RoI algorithms. This is intensified in mobile environments due to motion blur and long distances. DL models based on convolutional neural networks (CNNs) have demonstrated exceptional capability across computer vision tasks, including localization, tracking, and feature reconstruction. Among CNN models, You Only Look Once (YOLO) algorithms [27–30] have emerged as a state-of-the-art structure for real-time object detection and tracking.

In this study, we customized and trained a YOLO26n network [31–34] for LED detection and tracking under rolling-shutter and mobile conditions. To evaluate the model's performance, a dataset was collected from real daytime and nighttime environments under mobile conditions. The resulting dataset contained 1000 manually labeled images that encompassed both non-blurred and motion-blurred samples with different exposure times. The YOLO26n model included 7 to 9 convolutional layers for detection and tracking. The final layer used 42 filters to improve the feature extraction and classification accuracy. With the conventional RoI algorithm, we can obtain multiple white stripes instead of the LED position as with the DL model. By deploying the DL model, the communication performance can be enhanced in comparison with the RoI algorithm in a mobile environment. To evaluate the stability of the proposed system under the frame rate variation effect, we used some rolling-shutter camera models to verify the system's adaptability to different operating conditions. The use of different hardware platforms allowed for a comprehensive evaluation of the communication performance via multiple camera parameters. Furthermore, the use of camera models assisted with obtaining more representative datasets, thereby improving the detection performance. The YOLO model was trained on an NVIDIA GeForce RTX 3050 over 100 epochs. The YOLO26 model used input images with dimensions of 640 × 640 and a batch size of 16. The optimizer was AdamW, with a learning rate of 0.01. The dataset was divided into training, validation, and test datasets, with proportions of 70%, 15%, and 15%, respectively. The training results are shown in Figure 2. The proposed YOLO26n model attained good detection results (precision of 0.98, recall of ~0.97, F1-score of ~0.975, and $mAP_{50–95}$ of 0.875–0.88).

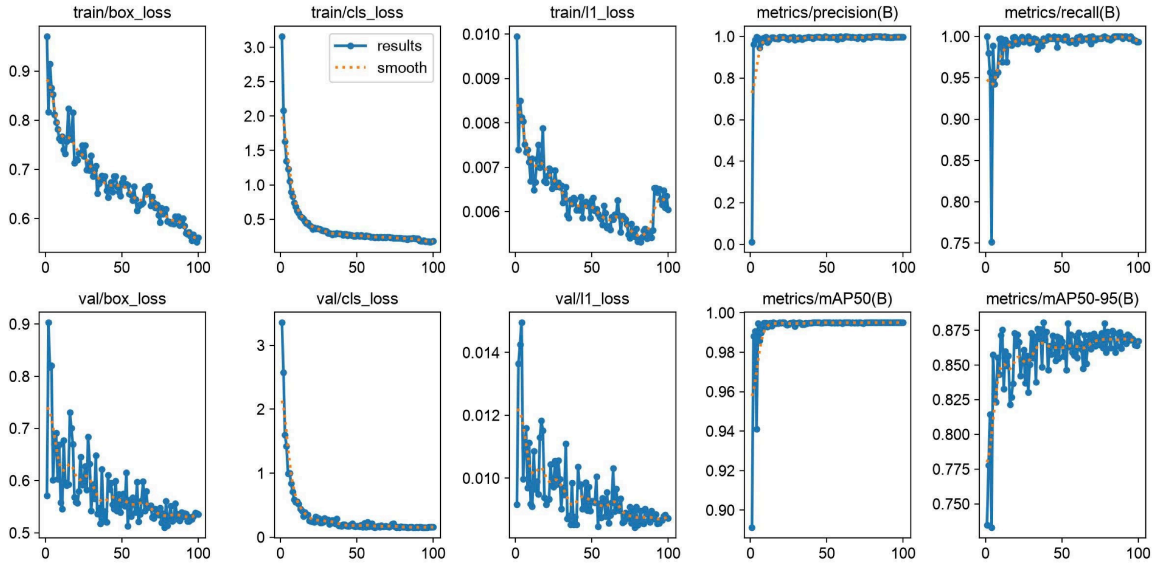

Figure 2. Object detection based on YOLO26n.

3.2. Denoising AutoEncoder for Data Decoding

The zeros-crossing method proposed in [21] determined the ON/OFF signal levels from the captured images. However, selecting an appropriate threshold became challenging under low-SNR conditions. As illustrated in Figure 3a, the method performs effectively over long transmission distances, where the SNR is relatively low. However, when the SNR value is low, the distinction between the ON and OFF states becomes clearer after the denoising autodecoder has processed the data. As shown in Figure 3b, we can see that the DAE can improve the signal by reducing the noise. As we mentioned above, over a long distance, the SNR reduces, and thus, there is difficulty in decoding the data, as shown in Figure 3a. Although the matched filter performs well in low-SNR environments, its effectiveness is significantly affected by image blur under mobile conditions. In particular, relative movement between the LED and camera introduces image blurring, which can lead to inter-symbol interference (ISI), and thus, degrade the performance of the OCC system. By applying a DAE, as shown in Figure 4, we can easily detect the threshold values, as shown in Figure 3b. However, it is difficult to accurately detect the threshold values in Figure 3a. Therefore, a DAE is helpful for the OCC decoder, especially in mobile environments and over long transmission distances. By employing a lightweight denoising autoencoder (DAE) tailored to an OCC system, the proposed system can improve the decoding performance while maintaining computational efficiency in harsh environments. Besides this, the proposed OCC system achieves a latency of less than 30 milliseconds, including the frame-gap time and decoder processing time.

After the LED detection, OCC waveforms were extracted from within the LED regions using YOLO26n. The C-OOK signals were collected by investigating the central region of each detected LED. The frame start position and threshold level for each LED were easily determined after the DAE [35] blocks, as shown in Figure 3b. Seven thousand images were collected with rolling-shutter cameras across different distances of 1, 5, 10, 15, 20, and 25 m and velocities of 0 to 3 m/s. To mitigate overfitting for the model, a relatively DEA system consisting of two hidden layers was employed in the encoder/decoder for the autoencoding denoising, as shown in Figure 4. When using more than five hidden layers for the DAE, the model appeared to overfit, which resulted in reduced precision on the dataset. A lightweight DAE tailored to the OCC system enhanced the decoding performance with low computational complexity. The lightweight DAE consisted of an

encoder, a latent representation, and a decoder. The encoder used ReLU activation to map a 100-dimensional input vector to 64 neurons, followed by a 32-dimensional latent representation. Using a 64-neuron hidden layer and a 100-dimensional linear output layer, the decoder recreated the initial input dimensions. The ReLU activation function was applied to the hidden layers. The model was trained using the MAE loss function and an Adam optimizer with a learning rate of 0.0001 and a batch size of 16. The dataset was divided into 70% for training, 15% for validation, and 15% for testing, with a batch size of 16. The model was trained on an NVIDIA GeForce RTX 3050 for 40 epochs. Figure 4 shows the autoencoding denoising (DAE) algorithm used to support decoding for long-range and mobile environments (velocity up to 3 m/s), which was designed to increase the OCC performance in mobile environments.

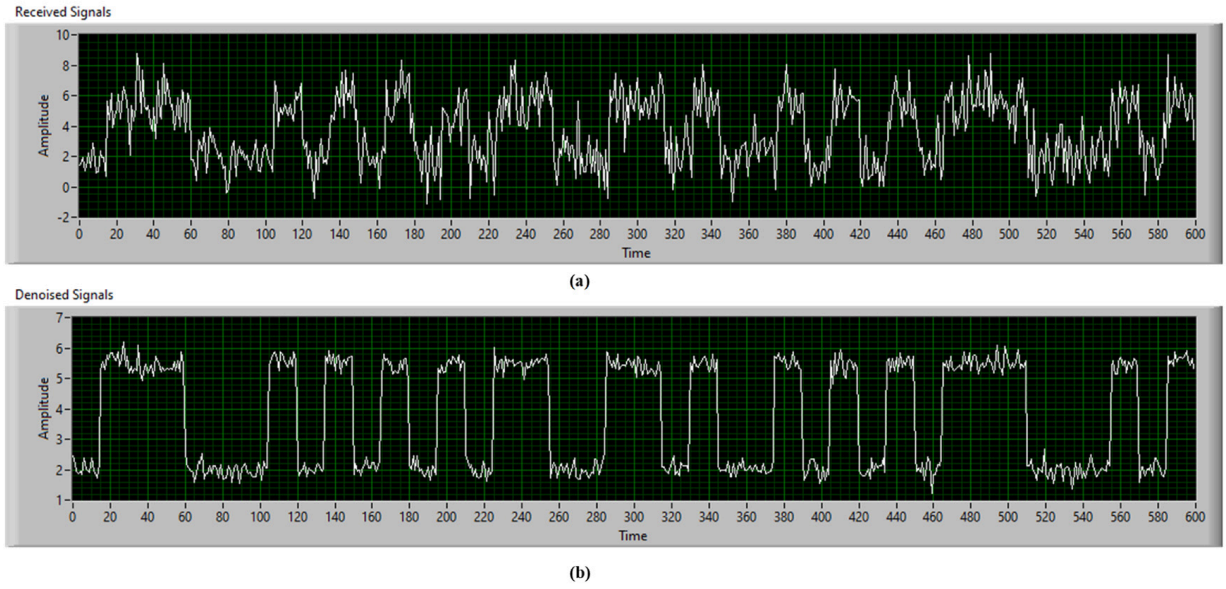

Figure 3. C-OOK signals over long distances (**a**) without DAE and (**b**) with DAE.

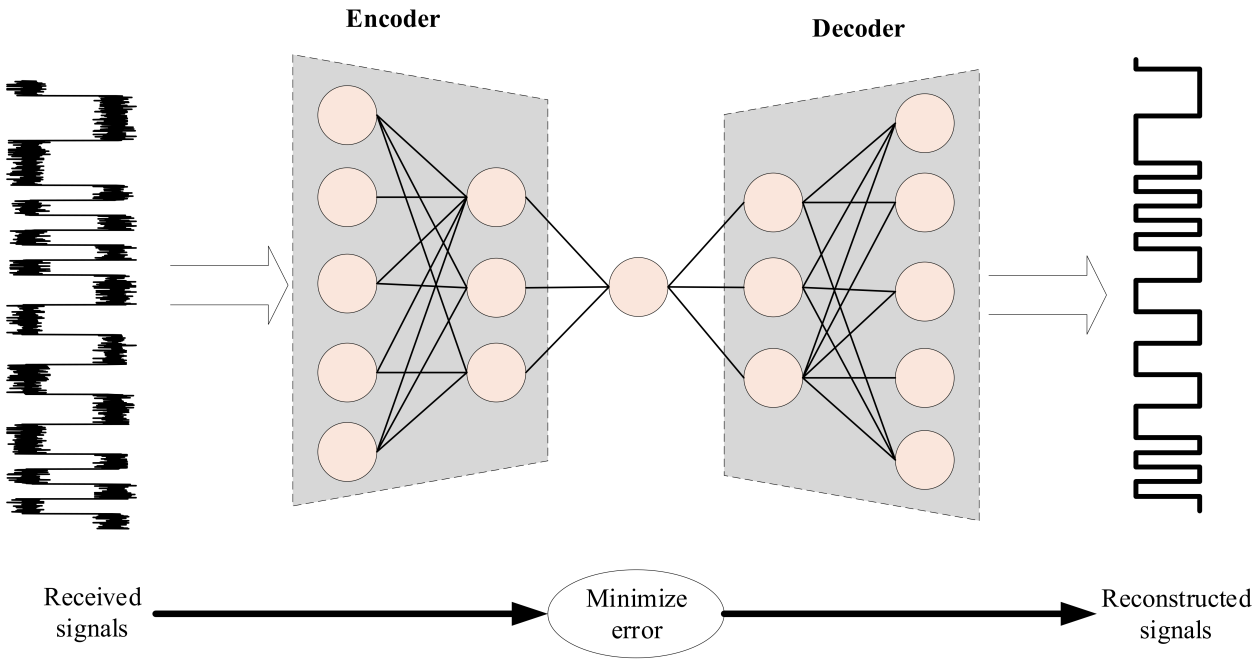

Figure 4. Autoencoding denoising with decoder.

4. Implementation Results

4.1. Fundamentals of OOK Modulation

Noise in a pixel can be modeled according to [21] as follows:

$$n \sim N(0, \delta(s)^2) \tag{1}$$

where s represents the pixel intensity; a noise variance was given as $\delta^2(s) = s.a.\alpha + \beta$, where a denotes the mark/space powers and α and β are fitting parameters. The pixel E_b/N_0 at the receiver side was given as follows:

$$Pixel\frac{E_b}{N_0} = \frac{E[s^2]}{E[n^2]} \approx \frac{a^2.\Delta}{a.\alpha.\Delta + \beta} \tag{2}$$

where E_b is the bit energy, N_0 is the noise power spectral density, and $\Delta = T_{exposure}/T_{bit}$ denotes the ratio between the camera exposure time and the bit duration. The parameters α and β are experimentally derived fitting constants that are determined when finding a relationship between the pixel intensity and pixel E_b/N_0 (Figure 5).

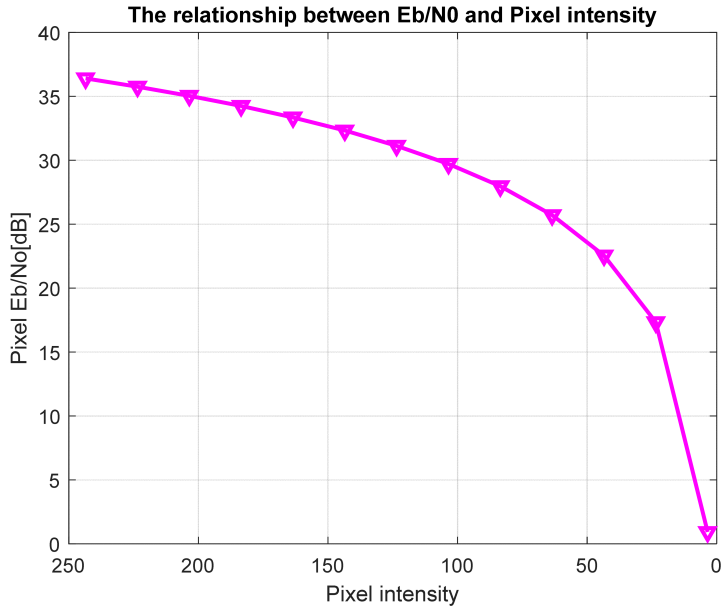

Figure 5. The correlation between pixel intensity and pixel Eb/N0.

4.2. Proposed System

Once the camera's frame rate is twice the transmitter's data packet rate, oversampling occurs, leading to support data redundancy and payload merging issues. To resolve the frame rate variation, a sequence number (SN) is inserted into each data sub-packet (DS). By evaluating the SNs in each packet, the receiver can remove duplicate packets with identical SNs and combine payloads with consecutive SN values (n − 1, n, n + 1), as shown in Figure 6a. Conversely, undersampling occurs when the camera frame rate drops below the transmitter's packet rate, resulting in missing packets. SNs enable missing packet detection by identifying non-sequential gaps in consecutive frames, as shown in Figure 6b. The number of packets that can be detected in the undersampling case depends on the SN length; for instance, a 3-bit SN can detect up to eight lost payloads. To evaluate the camera parameter impacts and optimize the SN length, the DAE network was deployed across multiple cameras with the C-OOK scheme. The quantized signal intensity profiles are detailed in Figure 7 with four-link setups, while Figure 8 depicts the receiver interface displaying real-time LED tracking with four links at the transmitter side, as well as the

decoded text output. After 7000 training iterations, the LED detection based on YOLO26n attained an average loss of approximately 0.11. Empirical field testing in daytime and nighttime environments using a velocity of 0–3 m/s demonstrated the viability of the proposed approach. As shown in Figure 9, the bit error rate versus communication distance of the DAE-assisted data decoding with and without the DAE were measured to show the effects of mobility. To gather the BER values in Figure 9, we deployed five times, and the reported BER is the average of five independent BER measurements.

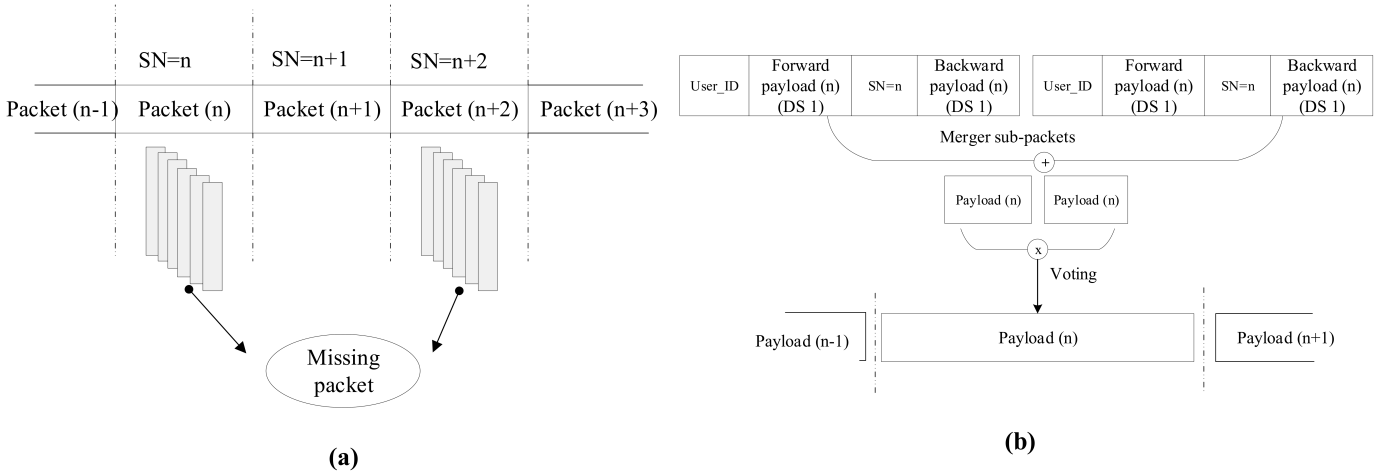

Figure 6. (**a**) Algorithm for detecting missing packets and (**b**) algorithm for packet merging.

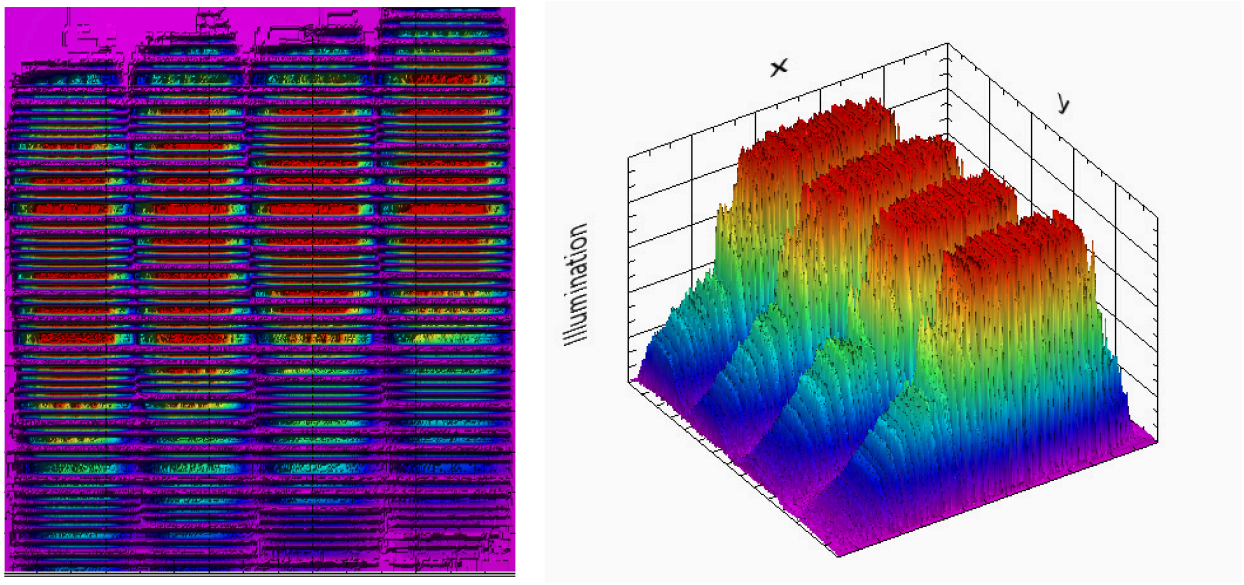

Figure 7. Quantized intensity profile of C-OOK signals with 4 links.

The experimental OCC setup operated at an optical clock rate of 10 kHz using Manchester line coding paired with Hamming code (15,11) and driving a transmitter array with 12 V, 3 W LEDs, and a size of (5 cm × 5 cm). Data were transmitted with 60 packages per second to match a rolling-shutter camera receiver (FL3-U3-13S2C-CS) operating at 60 frames per second (fps). We set up the implementation as follows: the distance between the four LEDs was 3 cm, the exposure time of the camera was 100 µs, and the LEDs/camera height was 1 m above the ground. The transmitter and receiver were aligned to establish a line-of-sight (LoS) link. During the implementation, the receiver was moved back and forth along the transmission direction. This configuration yielded peak uncoded and coded data

throughputs of 14.4 kbps and 10.56 kbps, respectively, when using the four link supports simultaneously. The BER performance was evaluated through five repeated physical experiments, and the reported BER values represent the average across these five independent experiments. As illustrated in Figure 9, evaluating the BER against the transmission distance confirms that the DAE-assisted decoder achieves a significant performance improvement over conventional decoders under identical camera settings and environmental conditions. While the throughput can be scaled by extending packet lengths or expanding the transmitter LED size, optical clock and packet rates must be jointly optimized with the camera specifications, communication range, and frame resolution to maintain continuity for the OCC connection. As shown in Figure 9, we can see that although the matched filter can work well at a low SNR, it does not perform well when moving due to the blur effect. Then, with the DAE, the BER value can be reduced compared with the matched filter (without the DAE). Regarding the target BER [36] of 10^{-3}, this was easily achieved with the DAE at a 15 m distance but without the DAE at a 7 m distance. The proposed deep learning architecture fulfills two stages: ensuring robust LED detection and assisting signal decoding to enhance the system performance in long-range and mobile environments. Specifically, the customized YOLO26n model achieves 98% detection accuracy when moving at 3 m/s with a four-link setup. A video demonstration of the system operating at 10 m is provided in the Supplementary Materials.

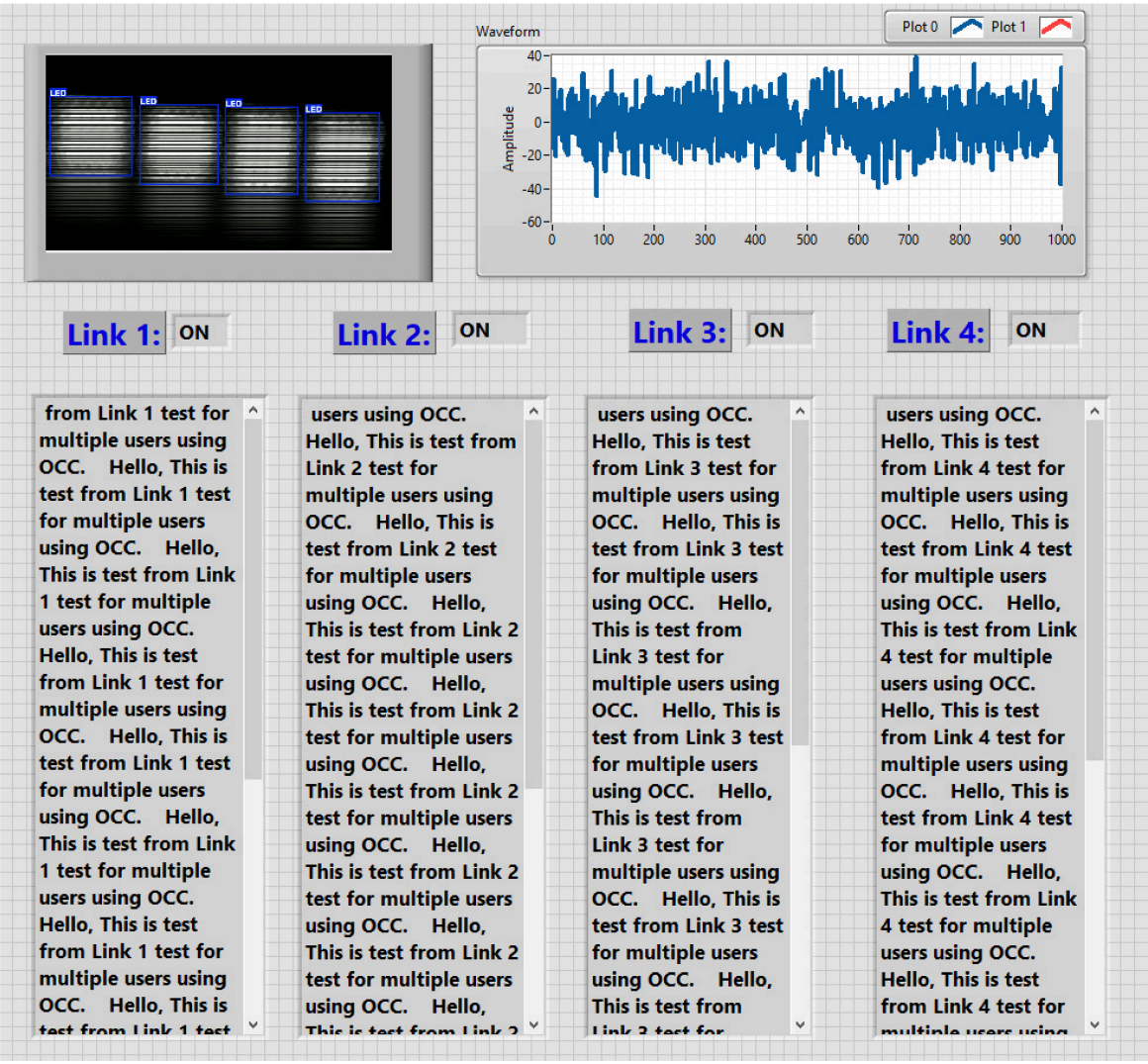

Figure 8. The receiver interfaces.

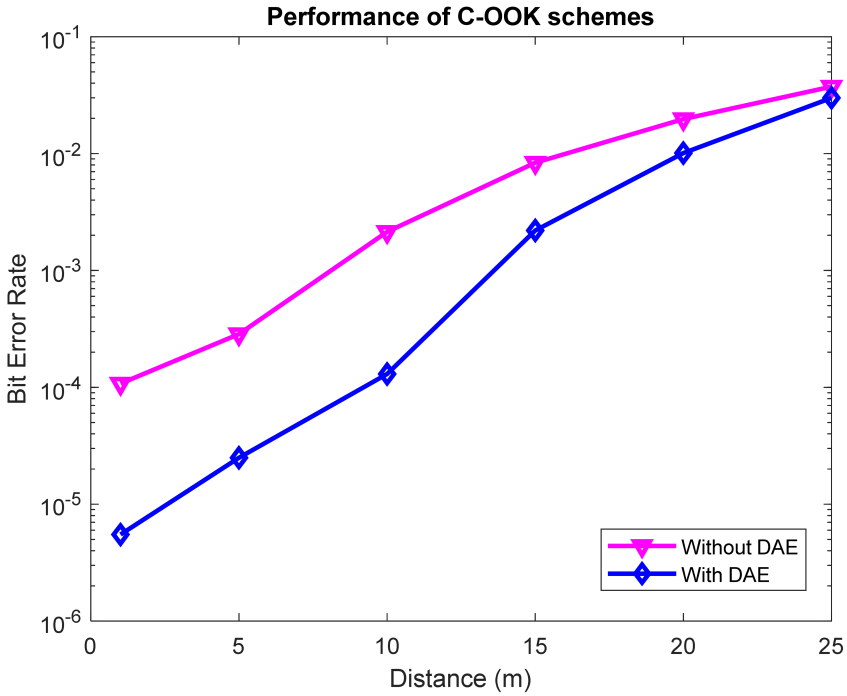

Figure 9. BER values of C-OOK scheme with/without the DAE decoder versus distance at a speed of 3 m/s.

5. Conclusions

This paper proposes an IoT-OCC system based on a C-OOK scheme for mobile environments. The proposed system applies deep learning for LED tracking and data decoding to reduce the bit error rate. To mitigate the effects of camera frame rate variations, sequence numbers (SNs) are inserted into each transmitted packet. The SNR increases as the exposure time increases; however, the system bandwidth decreases accordingly. Therefore, the exposure time should be carefully controlled. Furthermore, deep learning is employed to improve the system performance in mobile scenarios. The detection and tracking performance of the OCC system can be enhanced by applying YOLO26n instead of the conventional RoI-based approach. In addition, DAE-assisted data decoding demonstrates superior performance compared with conventional methods, particularly for long-distance transmission and in multi-user scenarios.

Supplementary Materials: The following supporting information can be downloaded from https://zenodo.org/records/21915002 (accessed on 10 September 2026): the supplementary material video shows the implementation of our proposed scheme at a distance of 10 m with four links.

Author Contributions: All authors contributed to this paper: H.N. proposed the idea and implementation methodology and revised the paper; L.C.N. reviewed and validated the work and edited the paper; N.H.N. supervised the work and provided funding support. All authors have read and agreed to the published version of the manuscript.

Funding: This research was funded by Hanoi University of Science and Technology (HUST) under project number T2025-PC-049.

Data Availability Statement: Restrictions apply to the datasets due to the project policy.

Conflicts of Interest: The authors declare no conflicts of interest.

References

1. Yalli, J.S.; Hasan, M.H.; Jung, L.T.; Yerima, A.I.; Aliyu, D.A.; Maiwada, U.D.; Al-Selwi, S.M.; Shaikh, M.U.R. A Systematic Review for Evaluating IoT Security: A Focus on Authentication, Protocols and Enabling Technologies. *IEEE Internet Things J.* **2025**, *12*, 18908–18928. [CrossRef]
2. Naeem, M.A.; Din, I.U.; Meng, Y.; Almogren, A.; Rodrigues, J.J.P.C. Centrality-Based On-Path Caching Strategies in NDN-Based Internet of Things: A Survey. *IEEE Commun. Surv. Tutor.* **2025**, *27*, 2621–2657. [CrossRef]
3. Hirata, A.; Laakso, I.; Apollonio, F.; Kodera, S.; Kubota, Y.; Lan, J.; Li, K.; Liberti, M.; Poljak, D.; Sasaki, K.; et al. Model Variability in Assessment of Human Exposure to Radiofrequency Fields. *IEEE J. Microw.* **2026**, *6*, 502–518. [CrossRef]
4. Nguyen, H.; Utama, I.B.K.Y.; Jang, Y.M. Enabling Technologies and New Challenges in IEEE 802.15.7 Optical Camera Communications Standard. *IEEE Commun. Mag.* **2024**, *62*, 90–95. [CrossRef]
5. Kour, H.; Jha, R.K.; Jain, S. Green and Safe 6G Wireless Networks: A Hybrid Approach. *IEEE Trans. Green Commun. Netw.* **2024**, *8*, 1729–1741. [CrossRef]
6. *IEEE Std 802.15.7-2011*; IEEE Standard for Local and Metropolitan Area Networks-Part 15.7: Short-Range Wireless Optical Communication Using Visible Light. IEEE-SA: Piscataway, NJ, USA, 2011.
7. *IEEE Std 802.15.7-2018*; IEEE Standard for Local and Metropolitan Area Networks—Part 15.7: Short-Range Optical Wireless Communications. IEEE-SA: Piscataway, NJ, USA, 2018.
8. Pathak, P.H.; Feng, X.; Hu, P.; Mohapatra, P. Visible light communication, networking, and sensing: A survey, potential and challenges. *IEEE Commun. Surv. Tutor.* **2015**, *17*, 2047–2077. [CrossRef]
9. Salmento, M.L.G.; Soares, G.M.; Alonso, J.M.; Braga, H.A.C. A Dimmable Offline LED Driver With OOK-M-FSK Modulation for VLC Applications. *IEEE Trans. Ind. Electron.* **2019**, *66*, 5220–5230. [CrossRef]
10. Zhang, X.; Xu, K.; Xu, N.; Li, W. Electromagnetic Interference Diagnosis of RF Circuits Based on Near Field Scanning. In Proceedings of the 2023 IEEE 7th International Symposium on Electromagnetic Compatibility (ISEMC), Hangzhou, China, 20–23 October 2023.
11. Tan, K.S.; Hinberg, I.; Wadhwani, J. Electromagnetic interference in medical devices: Health Canada's past current perspectives and activities. In *Proceedings of the IEEE International Symposium Electromagnetic Compatibility, Montreal, QC, Canada, 13–17 August 2001*; IEEE: Piscataway, NJ, USA, 2002; pp. 1283–1284.
12. Ong, Z.; Rachim, V.P.; Chung, W.Y. Novel electromagnetic-interference-free indoor environment monitoring system by mobile camera-image-sensor-based VLC. *IEEE Photonics J.* **2017**, *9*, 1–11. [CrossRef]
13. Haas, H.; Yin, L.; Wang, Y.; Chen, C. What is LiFi? *J. Light. Technol.* **2015**, *34*, 1533–1544. [CrossRef]
14. Ali, A.Y.; Zhang, Z.; Zong, B. Pulse position and shape modulation for visible light communication system. In *Proceedings of the International Conferences Electromagnetics Advanced Application, Palm Beach, FL, USA, 3–8 August 2014*; IEEE: Piscataway, NJ, USA, 2014; pp. 546–549.
15. Videv, S.; Haas, H. Practical space shift keying VLC system. In *Proceedings of the IEEE Wireless Communication Networking Conferences, Istanbul, Turkey, 6–9 April 2014*; IEEE: Piscataway, NJ, USA, 2014; pp. 405–409.
16. Deng, P.; Kavehrad, M. Real-time software-defined single-carrier QAM MIMO visible light communication system. In *Proceedings of the Integrated Communications Navigation and Surveillance (ICNS), Herndon, VA, USA, 19–21 April 2016*; IEEE: Piscataway, NJ, USA, 2016; pp. 5A3-1–5A3-11.
17. Cai, H.B.; Zhang, J.; Zhu, Y.J.; Zhang, J.K.; Yang, X. Optimal constellation design for Indoor MIMO visible light communications. *IEEE Commun. Lett.* **2016**, *20*, 264–267. [CrossRef]
18. Ayyash, M.; Elgala, H.; Khreishah, A.; Jungnickel, V.; Little, T.; Shao, S.; Rahaim, M.; Schulz, D.; Hilt, J.; Freund, R. Coexistence of WiFi and LiFi toward 5G: Concepts, opportunities, and challenges. *IEEE Commun. Mag.* **2016**, *54*, 64–71. [CrossRef]
19. Nguyen, H.; Imran, A.; Jang, Y.M. Survey of next-generation optical wireless communication technologies for 6G and Beyond 6G. *ICT Express* **2025**, *11*, 576–589. [CrossRef]
20. Nguyen, H.; Jang, Y.M. Experimental Demonstration of Deep Learning-Based HS2PSK-OFDM Scheme for Optical Camera Communication. *ICT Express* **2025**, *11*, 894–900. [CrossRef]
21. Luo, P.; Zhang, M.; Ghassemlooy, Z.; Zvanovec, S.; Feng, S.; Zhang, P. Undersampled-Based Modulation Schemes for Optical Camera Communications. *IEEE Commun. Mag.* **2018**, *56*, 204–212. [CrossRef]
22. *IEEE Std 802.15.7a-2024*; IEEE Standard for Local and Metropolitan Area Networks—Part 15.7: Short-Range Optical Wireless Communications Amendment 1: Higher Rate, Longer Range Optical Camera Communication (OCC), (Amendment to IEEE Std 802.15.7-2018). IEEE: Piscataway, NJ, USA, 2024.
23. Nguyen, V.H.; Thieu, M.D.; Nguyen, H.; Jang, Y.M. Design and Implementation of the MIMO–COOK Scheme Using an Image Sensor for Long-Range Communication. *Sensors* **2020**, *20*, 2258. [CrossRef] [PubMed]
24. Lin, H.; Si, J.; Abousleman, G.P. Region-of-interest detection and its application to image segmentation and compression. In Proceedings of the 2007 International Conference on Integration of Knowledge Intensive Multi-Agent Systems, Waltham, MA, USA, 30 April–3 May 2007.

25. Lin, G.-S.; Tuan, N.-M.; Chen, W.-J. Detecting region of interest for cadastral images in Taiwan. *Multimed. Tools Appl.* **2017**, *76*, 25369–25389. [CrossRef]
26. Cheng, Y.; Yang, P.; Zhang, N.; Hou, J. Edge-Assisted Lightweight Region-of-Interest Extraction and Transmission for Vehicle Perception. In *Proceedings of the 2023 IEEE Global Communications Conference, Kuala Lumpur, Malaysia, 4–8 December 2023*; IEEE: Piscataway, NJ, USA, 2024; pp. 1054–1059.
27. Isa, I.S.; Rosli, M.S.A.; Yusof, U.K.; Maruzuki, M.I.F.; Sulaiman, S.N. Optimizing the Hyperparameter Tuning of YOLOv5 for Underwater Detection. *IEEE Access* **2022**, *10*, 52818–52831. [CrossRef]
28. Diwan, T.; Anirudh, G.; Tembhurne, J.V. Object detection using YOLO: Challenges, architectural successors, datasets and ap-plications. *Multimed. Tools Appl.* **2023**, *82*, 9243–9275. [CrossRef] [PubMed]
29. Li, Y.; Zhang, X.; Wang, Z.; Wei, H. The Vanishing-Truth Patch: A Scale-Adaptive Vanishing Attack for Anchor-Based YOLO Detectors. *IEEE Geosci. Remote Sens. Lett.* **2026**, *23*, 6013305. [CrossRef]
30. Kaleem, Z. Lightweight and Computationally Efficient YOLO for Rogue UAV Detection in Complex Backgrounds. *IEEE Trans. Aerosp. Electron. Syst.* **2025**, *61*, 5362–5366. [CrossRef]
31. Thuan, L.D.; Ngan, N.T.H. OMR-Exam: An Efficient Lightweight Framework for Automated Exam Scoring via YOLO26, EfficientNet, and DCGAN-Enhanced Recognition. *IEEE Access* **2026**, *14*, 154198–154220. [CrossRef]
32. Liao, L.; Chen, L. YOLO26-Mamba3: Selective State Space With Complex State Space for Dense Railway Pedestrian Detection. *IEEE Signal Process. Lett.* **2026**, *33*, 3876–3880. [CrossRef]
33. Liu, M.; Deng, S. Lightweight Tomato Leaf Disease Detection via YOLO26 with MobileNetV4 Backbone and SimAM Attention. In *Proceedings of the 2026 International Conference on Sensor-Cloud and Edge Computing System (SCECS), Xuzhou, China, 2026*; IEEE: Piscataway, NJ, USA, 2026; pp. 144–148.
34. Gu, Y. CRP-YOLO26: A Lightweight Improved YOLO26 Algorithm for Small Object Detection in UAV Images. In *Proceedings of the 2026 5th International Conference on Artificial Intelligence, Internet of Things and Cloud Computing Technology (AIoTC), Nanchang, China, 17–19 July 2026*; IEEE: Piscataway, NJ, USA, 2026; pp. 683–689.
35. Alrayes, F.S.; Zakariah, M.; Amin, S.U.; Khan, Z.I.; Helal, M. Intrusion Detection in IoT Systems Using Denoising Autoencoder. *IEEE Access* **2024**, *12*, 122401–122425. [CrossRef]
36. Dong, X.; Zhang, K.; Zhang, J.; Yang, B.; Sun, C. Enabling gigabits-per-second underwater wireless optical communication with a Kramers–Kronig relation-based modulation scheme. *Opt. Lett.* **2025**, *50*, 5049–5052. [CrossRef] [PubMed]

Disclaimer/Publisher's Note: The statements, opinions and data contained in all publications are solely those of the individual author(s) and contributor(s) and not of MDPI and/or the editor(s). MDPI and/or the editor(s) disclaim responsibility for any injury to people or property resulting from any ideas, methods, instructions or products referred to in the content.